2-25-1999

Erratum: Lizards took express train to Polynesia (Nature (1999) 397 (13- 114)

C. Austin

correlated strongly with psychological and/or biological age so that geometrically feminized faces signal youthfulness more than biological femininity. If this were the case, then Perrett *et al.*'s observations would provide evidence for direct selection (for facial features signalling youthfulness), rather than against indirect selection (for secondary sexual characteristics signalling parasite resistance)[10].

It is no surprise that geometrical extrapolation may signal characteristics other than those from which they are constructed. The choice of initial features can be almost arbitrary and can produce unintended signals. For example, Fig. 1 shows an extrapolation along a pongid to a hominid skull continuum comparing and contrasting gorilla, *Paranthropus*, Neanderthal and human skulls. For our present purposes, note the delicate 'feminine' jaw and round 'neotenous' head. So the subjects studied by Perrett *et al.* might even be considered to be expressing a preference for 'hominized' over 'pongidized' faces.

To limit such spurious signals, we suggest that geometrical interpolation be used only to supplement biological data in constructing test faces: for example, to determine how subjects respond to age, averaged male and female faces could be prepared from sets of 15-year-old faces, from sets of 20-year-old faces, and so on. Ideally, averaged faces would represent a continuum of ages, but geometrical interpolation between closely spaced averages should be almost equivalent to a purely biological construction. Subjects could then be asked for their responses to these new facial subspaces.

The analogous experiment for biological sexuality is more difficult but still possible[11]: sex-hormone titres should be measured during development and averages prepared from sets of faces grouped according to time-integrated hormone amounts. Again, to reduce the data collection, one could interpolate between some reasonable number of averaged faces. Furthermore, the resulting shape continua would, by construction, reflect biological sexuality rather than the geometrical version used by Perrett *et al.*[1]. The biological age and sexuality shape continua could be compared to determine the correlation between the two signals.

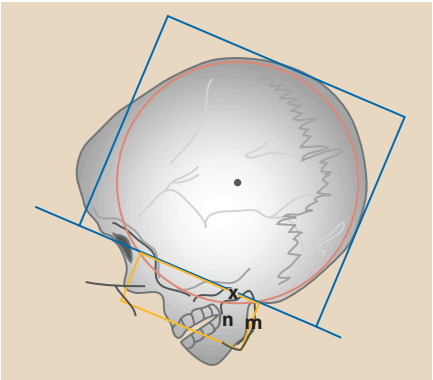

Figure 1 An extrapolation beyond human along a shape continuum defined by eight feature points on gorilla, *Paranthropus*, Neanderthal and human skulls. The subspace was constructed by hand (D.A.M.) using a procedure similar to, although considerably simpler than (that is, fewer skull features), the one followed by Perrett *et al.*[1]. (Courtesy of Marilyn Pettit archives.)

The biological determinant of the signal in such experiments would be unambiguous, isolating the psychological component of subjects' reactions to faces examined by Perrett *et al.*[1], and supporting an argument that is less dependent on questionable semantics.

David A. Meyer*, Melanie W Quong†
**Project in Geometry and Physics, Department of Mathematics 0112, and †Department of Biology 0366, University of California at San Diego, La Jolla, California 92093, USA*
e-mail:dmeyer@chonji.ucsd.edu

1. Perrett, D. I. *et al. Nature* **394,** 884–887 (1998).
2. Brennan, S. E. *Leonardo* **18,** 170–178 (1985).
3. Enquist, M. & Ghirlanda, S. *Nature* **394,** 826–827 (1998).
4. Folstad, I. & Karter, A. J. *Am. Nat.* **139,** 603–622 (1992).
5. Wedekind, C. *Proc. R. Soc. Lond. B* **247,** 169–174 (1992).
6. Hamilton, W. D. & Zuk, M. *Science* **218,** 384–387 (1982).
7. Grossman, C. J. *Science* **227,** 257–261 (1985).
8. Alexander, J. & Stimson, W. H. *Parasitol. Today* **4,** 189–193 (1988).
9. Zahavi, A. *J. Theor. Biol.* **53,** 205–214 (1975).
10. Kirkpatrick, M. & Ryan, M. J. *Nature* **350,** 33–38 (1998).
11. Thornhill, R. & Gangestad, S. W. *Hum. Nature* **4,** 237–269 (1993).

Perrett et al. *reply* — Our computer graphic manipulations of the 'geometrical' differences between male and female face shapes generate stimuli that embody the 'psychological' meaning of masculinity and femininity[1]. Meyer and Quong question whether our stimuli accurately imitate the 'biological' effect of sex hormones on facial structure, arguing that this should be defined from same-sex individuals whose levels of sex hormones differ.

As visible sexual dimorphism in the human face increases rapidly at puberty when sex steroids influence tissue growth, our working assumption is that the geometrical differences between male and female faces parallel the differences between individuals with high and low androgen levels. Masculinity in mammals is testosterone dependent, whereas femininity represents a more neutral developmental state[2]. Individuals with an XY chromosome pattern and complete androgen insensitivity syndrome have a female appearance. It is unlikely that geometrically 'feminizing' a face produces facial attributes associated with higher than average levels of androgens.

Meyer and Quong suggest that our subjects may be attracted to cues of youth rather than femininity in faces. Cues to femininity and youth are inextricably related, however, because of sex differences in the amount of facial growth at puberty. Pubescent male faces grow a great deal, whereas female faces change less and therefore remain relatively child-like. As we have shown[1], manipulations based on geometric sex differences in face shape alone affect apparent age. Certainly, face stimuli derived from males with measured high and low levels of testosterone would reflect androgenic effects on target tissues more accurately than our stimuli. Nevertheless, high-testosterone composite faces will carry more 'mature' features and may still appear older than low-testosterone composites.

Evolutionary theories do not predict that females should favour youthful-looking males; instead, they predict that cues to high male status, such as dominance, will be considered attractive[3]. Our masculinized male faces were rated as more dominant than feminized or average facial stimuli. Facial dominance is a predictor of male status in at least some human hierarchies[4] and yet subjects in our experiments preferred subdominant male faces. It is unclear whether this is due to a preference for youthfulness or a preference for other characteristics attributed to femininity (such as apparent warmth, kindness or a willingness to invest in progeny). What is apparent is that explanations of male attractiveness based on female sensory biases[5] or honest Zahavian handicaps fail to predict the preference for slightly feminized male facial characteristics.

Our investigation indicates that females select mates on characteristics other than, or in addition to, dominance.

D. I. Perrett, I. Penton-Voak
School of Psychology, University of St Andrews, Fife KY16 9JU, UK
e-mail: dp@st-and.ac.uk

1. Perrett, D. I. *et al. Nature* **394,** 884–887 (1998).
2. Owens, I. P. F. & Short, R. V. *Trends Evol. Ecol.* **10,** 44–47 (1995).
3. Buss, D. M. *Behav. Brain Sci.* **12,** 1–49 (1989).
4. Mueller, U. & Mazur, A. *Behav. Ecol.* **8,** 569–579 (1997).
5. Enquist, M. & Ghirlanda, S. *Nature* **394,** 826–827 (1998).

errata

In Christopher Austin's article "Lizards took express train to Polynesia" (*Nature* **397**, 113–114; 1999), the circles in Fig. 1 should have been blue and the squares should have been red, to be consistent with the figure legend.

The article "Josephson effect and a π-state in superfluid ^{3}He" by Olivier Avenel, Yury Mukharsky and Eric Varoquaux (*Nature* **397**, 484–485; 1999) should have contained the following reference list:

1. Pereverzev, S. V., Loshak, A., Backhaus, S., Davis, J. C. & Packard, R. E. *Nature* **388,** 449–451 (1997).
2. Backhaus, S., Pereverzev, S., Loshak, A., Davis, J. C. & Packard, R. E. *Science* **278,** 1435–1438 (1997).
3. Backhaus, S. *et al. Nature* **392,** 687–690 (1998).
4. Avenel, O. & Varoquaux, E. *Jpn. J. Appl. Phys.* **26,** (suppl.) 1798–1803 (1987).
5. Avenel, O. & Varoquaux, E. *Phys. Rev. Lett.* **60,** 416–419 (1988).

Lizards took express train to Polynesia

The pattern of human colonization of the islands of the central and eastern Pacific is contentious. Two models have been widely considered: the 'express train to Polynesia' and the 'entangled bank' hypotheses[1–4]. Here I analyse the mitochondrial DNA sequences of the lizard *Lipinia noctua*, which lives alongside humans on these Pacific islands, with a view to distinguishing between these two hypotheses. From a phylogenetic analysis of mitochondrial DNA sequence variation, I find that these lizards colonized the central and eastern Pacific as a result of human-mediated dispersal, presumably as stowaways on early Polynesian canoes. The extreme genetic similarity between the different colonies indicates rapid colonization from a single source, which I take as support of the express-train hypothesis.

The Pacific Ocean is the world's largest geographic feature, encompassing more area than all the continents combined, and the islands of the eastern Pacific were the last part of the world to be colonized by humans. The voyage to these islands has attracted attention because it could provide clues as to how human cultures evolved. The entangled-bank hypothesis[2] argues that movement into the central and eastern Pacific was a gradual event, occurring over an extended period from different Melanesian populations. In contrast, the express-train hypothesis[1] argues for rapid colonization from southeast Asia, with colonists moving through Melanesia and into the Pacific with little genetic exchange occurring between different groups.

Archaeological[5], linguistic[6] and genetic[7–9] data indicate that human migration from the Taiwan region to the Bismarck archipelago, northeast of New Guinea, occurred between 3500 BC and 1600 BC. The Lapita expansion, from the Bismarck islands into the central Pacific, is thought to have happened over a short period, perhaps only a few hundred years[1,3,5]. The further extension of humans into the eastern Pacific was slower, and the most remote regions were not reached until much later[4] (Fig. 1).

Lipinia noctua, a small lizard native to New Guinea, is a single species with one of the broadest distributions of any lizard. It occurs from the Papuan region throughout Oceania, to the Hawaiian islands in the northeast, and Easter Island and Pitcairn Island in the southeast. Because of the large ocean barriers and the morphological similarity between island populations, dispersal of the lizard from New Guinea was presumed to have been mediated by humans.

To investigate any potential congruent phylogeographic patterns between humans and this lizard, I collected mitochondrial DNA samples from 29 *L. noctua* lizards from 15 island populations (Fig. 1). From these samples, I sequenced and aligned a 300-base-pair portion of the gene encoding cytochrome *b* and analysed the results by maximum-parsimony and maximum-likelihood phylogenetic reconstruction methods using appropriate outgroups (Fig. 1).

The entangled-bank hypothesis predicts that *L. noctua* populations in the central and eastern Pacific should be paraphyletic (red and blue populations intermixed in Fig. 1) as a result of several dispersal events that reflect the different human migrations from Melanesia. The express-train hypothesis, however, predicts that *L. noctua* in the central and eastern Pacific should be monophyletic (red populations grouped together in Fig. 1) and show a high degree of genetic similarity because of a bottleneck associated with rapid human-mediated dispersal.

The colonization pattern for *L. noctua* matches the predictions of the express-train hypothesis (Fig. 1). All central and eastern Pacific populations of *L. noctua* form a monophyletic clade that differ by no more than two base-pair substitutions. As humans moved rapidly into the central Pacific, they could have inadvertently carried with them in their canoes a few lizards (or perhaps a single gravid female), causing the observed founder effect.

Although they are geographically part of Micronesia, the people of Kapingamarangi atoll are Polynesian in origin[4,6]. The *L. noctua* from there are also of the central/eastern clade, which strengthens the association between *L. noctua* and human colonization. The lizard populations from the central and eastern Pacific should be equally closely related to an original source population, presumably somewhere in the Bismarck or Solomon archipelagoes. However, this source population, identifiable by greater haplotype diversity, has not yet been sampled. When it is identified, it may reveal archaeological information about the early stages of the express train's journey. The populations of *L. noctua* in Micronesia show a large degree of genetic divergence, indicating that they are the result of pre-human natural dispersal[10].

The application of comparative phylogeography to evolutionary history, together

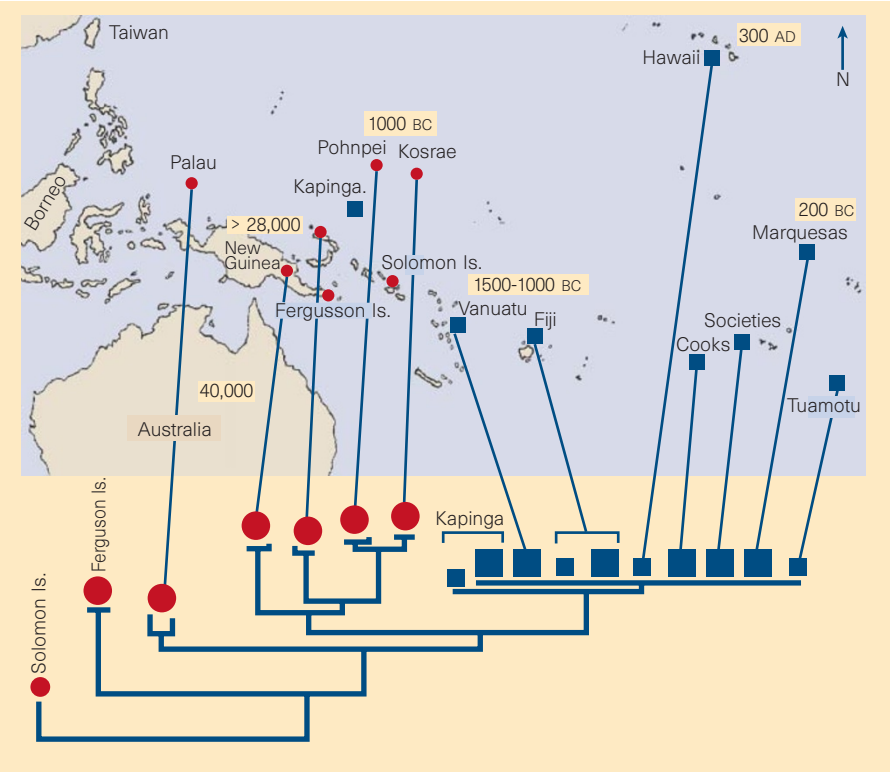

Figure 1 Maximum-parsimony phylogram for *Lipinia noctua*. Maximum-likelihood analyses produced the same topology. Symbol size represents sample size (small, $n=1$; large, $n=2$). Localities denoted by blue circles are all genetically distinct from one another (mean sequence divergence, 9.7%) and represent natural pre-human dispersal[10]. Localities denoted by red squares are genetically similar (mean sequence divergence, 0.008%) and represent human-mediated dispersal within the past 4,000 years. Kapinga indicates Kapingamarangi atoll. Dates represent approximate time of first human settlement[4]. (R. Fisher, J. Lum and D. Mindell, personal communication.)

with information about population structure from other such 'vagabond' fauna and flora, should continue to shed light on the vagaries of human evolution.

Christopher C. Austin
Evolutionary Biology Unit,
South Australian Museum,
Adelaide 5000, Australia
Present address: Institute of Statistical Mathematics,
4-6-7 Minami-Azabu Minato-ku,
Tokyo 106-8569, Japan
e-mail: caustin@ism.ac.jp

1. Diamond, J. M. *Nature* **336,** 307–308 (1988).
2. Terrell, J. *Antiquity* **62,** 642–657 (1988).
3. Clegg, J. B. *Lancet* **344,** 1070–1071 (1994).
4. Bellwood, P. S. in *The Colonization of the Pacific: Some Current Hypotheses* (eds Hill, A. V. S. & Serjeantson, S. W.) 1–59 (Oxford Univ. Press, 1989).
5. Kirch, P. V. & Hunt, R. L. *Radiocarbon* **30,** 161–169 (1988).
6. Pawley, A. & Green, R. *Ocean Ling.* **12,** 1-67 (1973).
7. Hagelberg, E. & Clegg, J. B. *Proc. R. Soc. Lond. B* **252,** 163–170 (1993).
8. Redd, A. J. *et al. Mol. Biol. Evol.* **12,** 604–615 (1995).
9. Martinson, J. J. in *Molecular Biology and Human Diversity* (eds Boyce, A. J. & Mascie-Taylor, C. G. N.) 171–195 (Cambridge Univ. Press, 1996).
10. Thorpe, R. S., McGregor, D. P., Cumming, A. M. & Jordan, W. C. *Evolution* **48,** 230–240 (1994).

The first true inorganic fullerenes?

Boron nitride and materials of composition MX_2, where M is molybdenum or tungsten and X is sulphur or selenium, can form fullerene-like structures such as nested polyhedra or nanotubes[1–3]. However, the analogy to the carbon fullerene family[4] falls short because no small preferred structure akin to C_{60} (ref. 5) has been found. We have discovered nano-octahedra of MoS_2 of discrete sizes in soots that we prepared by laser ablation of pressed MoS_2 targets. These nano-octahedra are much larger than C_{60} structures, having edge lengths of about 4.0 and 5.0 nanometres, and may represent the first 'inorganic fullerenes'.

Targets were prepared by pressing 98% pure MoS_2 powder and ablated using a KrF pulsed excimer laser (8 Hz, 248 nm, ~300 mJ per pulse, ~20 ns per pulse, ~10 J cm^{-2}) under flowing helium or argon (500–800 torr, ~90 cm^3 min^{-1}). The beam was moved every 4 minutes during the 20-minute runs to strike fresh target material, with the chamber and target temperature ranging from 30 to 600 °C. The soot generated was collected, ultrasonicated in acetone, and applied to a grid for imaging by transmission electron microscopy (TEM).

Soot produced between 30 and 500 °C contained crystalline and amorphous MoS_2 fractions, as well as smaller rhomboidal, rectangular and hexagonal structures 3 to 5 nm long with two or three layers. The crystalline material included large sheets and tubes and a variety of nested polyhedra 15 to 35 nm long that were similar to those produced previously[6]. Above 550 °C, only crystalline folded sheets of MoS_2 were produced.

TEM stage-tilting experiments on 30 two- and three-layered structures showed that the small rhomboids, rectangles and hexagons were different projections of the same three-dimensional structure: an octahedron (Fig. 1a). The TEM image for a closed three-layer structure changes with tilts of 10° and 20° (Fig. 1b). The image at 0° is the projection expected for an octahedron orientated such that only two triangular faces are seen. When it is tilted, the projection changes, resulting in a nearly rectangular projection at 20°. Stick models depicting how an octahedron's projection changes with tilting are also shown in Fig. 1b. The model octahedron was orientated to project a match to the 0° image, and the model was then tilted with the same axis used in the TEM. Many other TEM tilt sequences could also be generated with projections of a model octahedron. In some cases, slight movements of the particles on the TEM grid ruined the correlation, but individual images could still be represented by the projection of an octahedron.

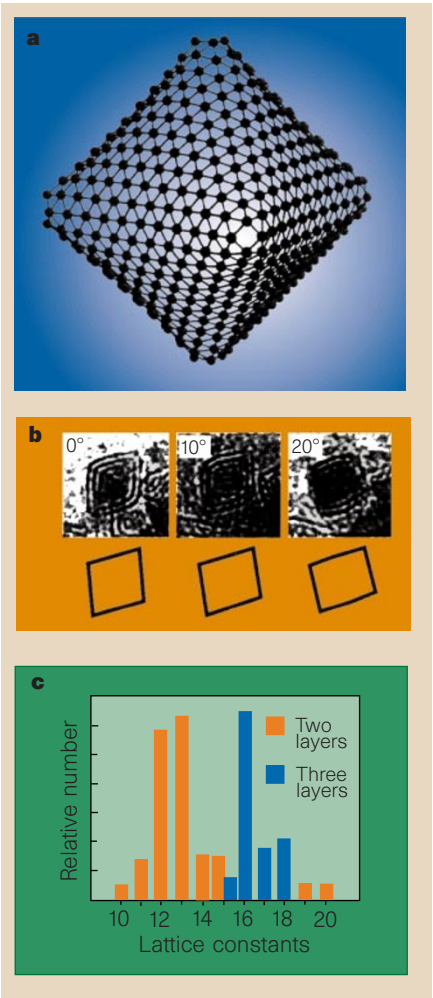

Figure 1 Structure of the molecules. **a,** Model octahedron with an edge length of 12 *a* lattice constants showing only the molybdenum sublattice. **b,** Transmission electron microscope images and model-generated projections for a three-layer MoS_2 rhomboid at 0° and undergoing tilts of 10° and 20°. **c,** Histogram of octahedral edge lengths in *a* lattice constants determined from 30 rhomboidal, rectangular and hexagonal projections observed by TEM.

The edge length of the octahedron may be calculated from TEM projections, assuming a regular octahedral structure. A histogram of edge lengths for 30 different structures is shown in Fig. 1c. Two pronounced peaks are seen at 12–13 and 16 times the *a* lattice constant (the Mo–Mo distance, 3.16 Å) of MoS_2 for two- and three-layer species, respectively. The spacing between the layers is about 0.6 nm, in good agreement with the interlayer spacing in bulk MoS_2. The edge of the three-layer species is about four *a* lattice constants larger than that of the underlying two-layer structure, exactly the size required to maintain the bulk interlayer spacing.

Although the reasons for these specific sizes are not clear, a preference for two- and three-layer structures may be associated with the two- and three-layer polytypes[7]. The octahedral shape might be anticipated for a closed MoS_2 structure as the triangular faces share the symmetry of the trigonal Mo and S sublattices. Rounded corners and edges are also expected for MoS_2 sheets, which cannot be severely bent without strain. Energy-dispersive spectroscopy indicated a Mo:S ratio of about 1:2 with no detectable impurities. Satisfying such a ratio exactly is impossible in an octahedron, but several arrangements come close. For example, the Mo–S coordination could remain trigonal prismatic, as in the bulk form, with a given face being slightly rich or poor in sulphur. The structure at the vertices is unclear, but either a four-membered Mo ring[3] or a single Mo atom might be stable (B. Parkinson, personal communication).

TEM measurements could be performed only on nano-octahedra that were separated from the agglomerates formed on the TEM grid. Consequently, we cannot yet estimate the density of nano-octahedra in the laser-generated soots. We are purifying these inorganic fullerenes so that we can ascertain their properties, and are also finding out whether similar cage structures can be made using other layered materials.

P. A. Parilla, A. C. Dillon, K. M. Jones, G. Riker, D. L. Schulz, D. S. Ginley, M. J. Heben
National Renewable Energy Laboratory,
1617 Cole Boulevard, Golden,
Colorado 80401-3393, USA

1. Tenne, R., Margulis, L., Genut, M. & Hodes, G. *Nature* **360,** 444–446 (1992).
2. Chopra, N. G. *et al. Science* **269,** 966–967 (1995).
3. Tenne, R. *Adv. Mater.* **7,** 965–995 (1995).
4. Kroto, H. *Science* **242,** 1139–1145 (1988).
5. Kroto, H. W. *et al. Nature* **318,** 162–163 (1985).
6. Feldman, Y., Wasserman, E., Srolovitz, D. J. & Tenne, R. *Science* **267,** 222–225 (1995).
7. Wilson, J. A. & Yoffe, A. D. *Adv. Phys.* **18,** 193–335 (1969).

two others with "eye lotion to be dispersed, good for eyesight". Analysis[8] has shown that the former product was galena and the latter were mixtures of lead chloride and carbonate. Moreover, Egyptian medical papyrus lists one hundred recipes for treating problems of the eyelids, iris and cornea, as well as trachoma and conjunctivitis. Some of these materials have been identified as malachite, galena and their derivatives, although several others have not yet been identified[9].

Fire-based technology has been used to manufacture Egyptian blue pigments since about 2500 BC (refs 1,2). We have now shown that wet chemistry was used as long ago as 2000 BC. This finding shows that the chemical technology of Ancient Egypt was more sophisticated than previously thought.

P. Walter*, P. Martinetto*, G. Tsoucaris*, R. Bréniaux†, M. A. Lefebvre†, G. Richard†, J. Talabot†, E. Dooryhee‡

**Laboratoire de Recherche des Musées de France, UMR 171-CNRS, 6 rue des Pyramides, 75041 Paris Cedex 1, France*
e-mail : p.walter@culture.fr
†L'Oréal-Recherche, 90 rue du Général Roquet, 92583 Clichy Cedex, France
‡European Synchrotron Radiation Facility, BP 220, 38043 Grenoble Cedex, France

1. Forbes, R. J. *Studies in Ancient Technology* Vol. III (Brill, Leiden, 1955).
2. Lucas, A. & Harris, J. R. *Ancient Egyptian Materials and Industries* 80–97 (Arnold, London, 1963).
3. Vandier d'Abbadie, J. *Catalogue des objets de toilette égyptiens du Musée du Louvre* (Réunion des Musées Nationaux, Paris, 1972).
4. Edwards, R., Gillard, R. D., Williams, P. A. & Pollard, A. M. *Mineral. Mag.* **56,** 53–65 (1992).
5. Conophagos, C. in *The Evolution of the First Fire-Using Industries* (eds Wertime, T. A. & Wertime, S. F.) 181–191 (Smithsonian Institution Press, Washington DC, 1982).
6. Wellman, M. *Dioscoridis Pedanii, de Materia Medica, Libri Quinque* (Weidmannsche, Vienna, 1958).
7. Zehnacker, H. *Pline l'Ancien, Histoire Naturelle* XXXIII (Belles Lettres, Paris, 1983).
8. Lucas, A. in *Quibell Ann. Serv. Antiq. Egypte* **2,** 141–143 (1901).
9. Bardinet, T. *Les papyrus médicaux de l'Egypte pharaonique* (ed. Fayard, Paris, 1995).

Supplementary information is available on *Nature*'s World-Wide Web site (http://www.nature.com) or as paper copy from the London editorial office of *Nature*.

Josephson effect and a π-state in superfluid ^{3}He

Evidence has been reported for Josephson-type behaviour in the flow of superfluid helium-3 (^{3}He) through an array of 4,225 apertures[1,2] and for a metastable π-state at low temperature[3]. Here we show that an array of holes cannot be expected to act as a single weak link in such a system, and that these results can be explained without invoking the superfluid analogue of the much-debated 'π-junction' in other systems.

Convincing experimental evidence for the Josephson effect in superfluid ^{3}He was first reported ten years ago[4,5]. The mass current J and the quantum-mechanical phase difference $\Delta\phi$ across a single microscopic orifice are well represented by the relations $J = J_c \sin\zeta$, and $\Delta\phi = \zeta + \alpha\sin\zeta$, where J_c is the critical current, ζ is an auxiliary phase angle and α is a non-ideality parameter. These relations describe both the ideal Josephson regime, $\alpha \approx 0$, observed close to the superfluid transition temperature, and the phase-slippage regime, $\alpha > 1$, which occurs at lower temperatures. This relation is represented by the solid line in Fig. 1a for $\alpha = 2$. In this hysteretic regime, the current is double-valued around $\Delta\phi = \pi$. In an array of holes, if half of the holes sit on the upper branch, J_+, and the other half sit on the lower one, J_-, the measured current through the array is $(J_+ + J_-)/2$, as represented by the dotted line in Fig. 1a. Numerical simulations indicate that a suitable excitation drive can set an array of holes into this state.

The time evolution of the membrane displacement, X, monitoring the flow through an array of N apertures, is obtained by solving numerically the set of equations

$$\Delta\phi = \zeta_i + \alpha_i \sin\zeta_i, \quad (1)$$

$$dX/dt = C \sum_{i=1}^{N} \sin\zeta_i, \quad (2)$$

$$\frac{d(\Delta\phi)}{dt} = V\sin(\omega t) - X - \frac{1}{\omega_0 Q}\frac{dX}{dt} \quad (3)$$

where C is related to the small signal oscillation frequency, $\omega_0^2 = C\sum_{i=1}^{N}(1/1+\alpha_i)$, $V\sin(\omega t)$ is the external drive of maximum amplitude V at frequency ω, and Q is the quality factor of the resonator.

The result of such a simulation is shown in Fig. 1b. We used 200 holes with a gaussian distribution of α_i values with mean value 2 and standard deviation 0.1. Apertures in different regions of the array experience different series hydraulic inductances, and the spread in α_i in the previous experiments[1–3] could actually be larger. The Q value of the resonator was set at 1,000. The external drive, $Vex = V\sin(\omega t)$ in equation (3), was made of four periods at a frequency $\omega = 1.1\omega_0$ and the amplitude was adjusted until a stable low-amplitude state was reached. In this state, about half of the holes have experienced a phase slip. The kinetic energy is then stored in the circulating currents in the array and a small perturbation can drive the system out of this state, in one direction or in the other, as shown in Fig. 1b for a positive perturbation.

A plot of $d(\Delta\phi^*)/dt$, defined as $-X(t)$, versus $\Delta\phi^*$, defined as $-\int_0^t X(t)dt$, is represented in Fig. 1c. According to equation (3), these $\Delta\phi^*$ are not the true $\Delta\phi$, but such a procedure was used to plot Fig. 3a in ref. 3,

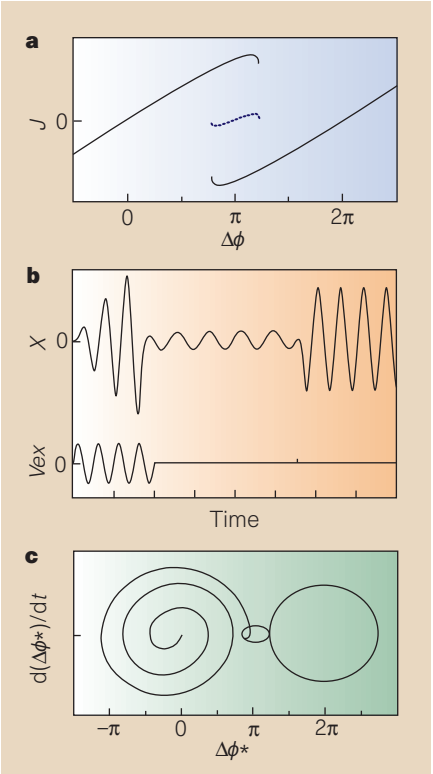

Figure 1 Numerical simulations. **a,** Current–phase relationship for $\alpha = 2$. Dotted line, artefact of the measurements in an array of holes discussed in the text. **b,** Time evolution of the membrane amplitude X in response to an external drive Vex. **c,** Corresponding trajectory in the $d(\Delta\phi^*)/dt$ versus $\Delta\phi^*$ plane.

with which our numerical data must be compared. The agreement with real data is striking, taking into account that there is neither noise nor filtering in the simulated data.

With these input parameters, the excitation window leading to a stable low-amplitude state is very narrow. Slight variations in the distribution of α_i, in the shape of the applied drive, or in the details of the current–phase relationship around π could widen this window.

In conclusion, our analysis shows that direct measurements of the current–phase relationship in an array of holes should be interpreted with care. The data in refs 1–3 can be reproduced by simple numerical simulations that involve only physical mechanisms previously demonstrated to take place in a single aperture. By themselves, these data do not reveal the existence of an exotic π-junction, hidden degrees of freedom, or any influence of textural effects.

Olivier Avenel*, Yury Mukharsky*, Eric Varoquaux†

**CEA-DRECAM, Service de Physique de l'État Condensé, Centre d'Etudes de Saclay, 91191 Gif-sur-Yvette Cedex, France*
e-mail : avenel@spec.saclay.cea.fr
†CNRS-Laboratoire de Physique des Solides,

Bât. 510, Université Paris-Sud,
91405 Orsay, France

Backhaus et al. *reply* — Avenel *et al.* have suggested a mechanism that might explain the recently discovered[1] metastable π-state in a superfluid ^{3}He weak-link array. We are pleased that our experiment is leading to new ideas that may extend the understanding of weak-link arrays. We agree with Avenel *et al.*'s comment that, when the individual apertures are in a (short coherence length, low temperature) hysteretic regime, collective phenomena quite distinct from single weak-link behaviour might be observed. Nevertheless, in the temperature regime in which the coherence length is comparable to the aperture dimensions, we have shown that the collective behaviour of the array is similar to that of a single weak link[2,3].

Although we are gratified that the mechanism proposed by Avenel *et al.* for the π-state expands on our previous conjecture[1] that internally trapped circulating currents could be involved in its existence, we do not believe that it is the only possible explanation. This is because agreement between a given data set and a numerical simulation, using a model with several adjustable parameters, represents a check that the model is consistent with the data, but does not qualify as a proof of the model[4]. Therefore, we cannot say to what extent their model represents physical reality better than other theories of the π-state that have been recently proposed[5].

However, several aspects of their simulation disagree with our experimental observations. In particular, the model presented by Avenel *et al.* does not seem to conserve energy in the oscillator, contrary to our experimental results. Their model predicts that the $I(\phi)$ relation should extend beyond $\phi=\pi$ before the onset of the π-state. In contrast, the collapse into the π-state occurs at $\phi<\pi$. Finally, as shown in their Fig. 1c and supported by our own simulations, their model leads to metastable states at positions other than π, a feature also in contradiction to the data.

We hope that Avenel *et al.* will continue to refine their simulations to make predictions that could lead to a conclusive test of their underlying model.

S. Backhaus, R. W. Simmonds, A. Loshak, J. C. Davis, R. E. Packard
Department of Physics,
University of California, Berkeley,
Berkeley, California 94720, USA

1. Backhaus, S. *et al. Nature* **392,** 687–690 (1998).
2. Pereversev, S. V., Loshak, A. Backhaus, S., Davis, J. C. & Packard, R. E. *Nature* **338,** 449–451 (1997).
3. Backhaus, S., Pereversev, S., Loshak, A., Davis, J. C. & Packard, R. E. *Science* **278,** 1435 (1997).
4. Varoquaux, E., Avenel, O., Ihas, G. & Salmelin, R. *Physica B* **178,** 309–317 (1992).
5. Hatakanaka N. *Phys. Rev. Lett.* **81,** 17 (1998).

How and why a parasitic nematode jumps

Jumping is an unusual behaviour performed by some nematode species[1], but has been seen only in the infective or phoretic stages of species associated with insects[1–3]. This correlation suggests that jumping may be involved in the location of insect hosts. We find that infective juveniles of the insect-parasitic nematode *Steinernema carpocapsae*, when standing on their tails, are triggered to jump by the presence of host-associated volatile cues, and that they tend to jump towards them. Directional jumping in response to information about insect proximity could be an adaptation for host attack by this parasite.

S. carpocapsae is a lethal endoparasite capable of infecting a broad range of insect species[4]. The infective juvenile, which emerges from a depleted host cadaver to seek out a new insect to infect, is the only free-living stage. Infective juveniles tend to be found at the soil surface[5], and use an ambushing search strategy in which they stand on their tails and attach to a passing insect[2]. They are more likely to be picked up by an insect when they are standing because of the reduced surface tension holding them to their substrate.

Jumping, which previously was inaccurately described[1], is initiated when a standing nematode quickly bends the anterior half of its body until its head region makes contact with the ventral side of its body. The two body regions appear to be held together by the film of water covering the nematode's body[1]. The nematode now has resistance to the bending of its body, so it can use its normal sinusoidal crawling behaviour to slide its body in a posterior direction, causing the loop to become progressively smaller and the bend in its body to become more acute.

Eventually, the body becomes so contorted that the cuticle on the dorsal side becomes extremely stretched and the cuticle on the ventral side kinks, generating sufficient force to break the surface tension forces holding the nematode to the substrate and propel it through the air. The forces generated by this jumping mechanism are sufficient to propel nematodes an average distance of 4.8 ± 0.8 mm (nine times the nematode's body length) and an average height of 3.9 ± 0.1 mm (seven times the nematode's body length).

If jumping behaviour has been acted on by natural selection to function in finding hosts by ambush, then we might expect it to be triggered by the presence of potential hosts, and for nematodes to jump towards the host. We found that *S. carpocapsae* infective juveniles standing on their tails responded differently to different types of information from the environment (Fig. 1). Nonspecific cues such as air movement, in this case associated with moving a syringe tip to within a millimetre of the infective juvenile or applying a puff of air through the syringe, triggered a small increase in jumping. The proportion of individuals jumping increased dramatically when more specific cues indicating the proximity of an insect were introduced. When the tip of a syringe containing larvae of the host *Galleria mellonella* (Lepidoptera) or adults of *Acheta domesticus* (Orthoptera) was introduced to standing infective juveniles, nearly all nematodes were induced to jump.

S. carpocapsae infective juveniles were able to change the direction of jumping in response to information from the environment (Fig. 1). Infective juveniles tended to jump towards the source of the air movement when air movements were small (syringe), but directionality was lost when they were large (puff of air), indicating that large air movements may inhibit the nematode from deriving directional information. When host cues were present, the nematodes tended to jump towards the source of the cues; however, there seem to be two

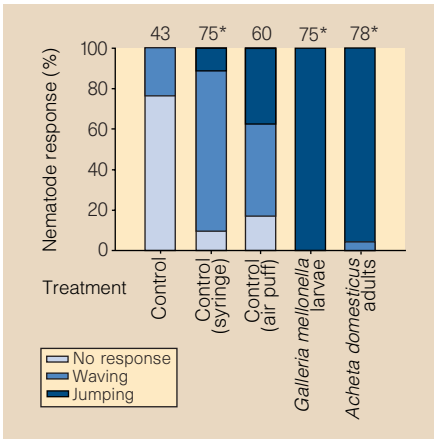

Figure 1 Influence of different cues on the initiation and direction of jumps of *Steinernema carpocapsae* infective juveniles. The following stimuli were presented by moving a Hamilton 10-ml gas-tight syringe to within 1 mm of a standing infective juvenile: control (no syringe); syringe (empty syringe); air puff (syringe was depressed to create a puff of air); or the syringe contained four individuals of either *Galleria mellonella* larvae or *Acheta domesticus* adults. Nematodes either remained in the straight standing posture (no response), waved back and forth while standing (waving), or initiated a jump (jumping). The proportion of individuals jumping towards the cues is shown at the top of each bar; numbers with stars are significantly different in jumping direction (contingency table analysis with chi-square tests at $P<0.05$). We tested 60 nematodes for each treatment.